This version is available at http://strathprints.strath.ac.uk/58492/

COLLISION AVOIDANCE AS A ROBUST REACHABILITY PROBLEM UNDER MODEL UNCERTAINTY

Massimiliano Vasile[*], Chiara Tardioli[†], Annalisa Riccardi[‡] and Hiroshi Yamakawa[§]

The paper presents an approach to the design of an optimal collision avoidance maneuver under model uncertainty. The dynamical model is assumed to be only partially known and the missing components are modeled with a polynomial expansion whose coefficients are recovered from sparse observations. The resulting optimal control problem is then translated into a robust reachability problem in which a controlled object has to avoid the region of possible collisions, in a given time, with a given target. The paper will present a solution for a circular orbit in the case in which the reachable set is given by the level set of an artificial potential function.

INTRODUCTION

In this work, the problem of avoiding the collision of a controlled object with an uncontrolled target object is translated into a robust reachability problem. The dynamics of the controlled object is assumed to be affected by uncertainty in the dynamic model itself. In orbit determination, a commonly used approach to capture unmodelled accelerations is to introduce so called *empirical accelerations* as additional components to the dynamics. The value of these empirical accelerations can be defined in a number of different ways exploiting the available measurements.

It is customary to use time series expansions in polynomial or trigonometric form whose coefficients need to be found by matching the predication of the model with the observations.[1] Another approach is to treat empirical accelerations as stochastic processes that can be reconstructed by an approach using a Kalman type of sequential filtering.[2]

All these techniques generally work satisfactorily and allow one to work with a reduced dynamics without the need for extremely high fidelity models. On the other hand, they do not immediately furnish a functional representation of the missing components. Even using time series expansions, which are valid within the interval in which the measurements are available, to extrapolate the behavior of the dynamical system does not always lead to the desired results. Furthermore, time series do not provide information on the dependency of the empirical accelerations on any of the state variables.

[*]Professor, Department of Mechanical & Aerospace Engineering, University of Strathclyde, 75 Montrose Street, Glasgow, UK.
[†]PhD candidate, Department of Mechanical & Aerospace Engineering, University of Strathclyde, 75 Montrose Street, Glasgow, UK.
[‡]KE Fellow, Department of Mechanical & Aerospace Engineering, University of Strathclyde, 75 Montrose Street, Glasgow, UK.
[§]Professor, Research Institute for Sustainable Humanosphere, Kyoto University, Uji Campus, Uji, Kyoto, Japan.

For this reason in this paper it is proposed to use polynomial expansions of the state variables instead. The approach proposed in this paper is reminiscent of the approach used in multifidelity modeling to capture model uncertainty via discrepancy functions. As an example in Ng and El-dred,[3] the discrepancy is modeled with a polynomial chaos expansion under the assumption that the missing component is a stochastic process. Under the same assumption of stochastic unmodelled component, Gaussian mixtures were proposed to capture the distribution of the propagated states.[4] In this paper, instead, the missing component in the model is considered to be due to a deterministic process that is only partially observable, or it is observable with some uncertainty.

Once the uncertainty in the dynamic model is quantified, the design of an optimal collision maneuver is translated into a robust reachability problem[5] in which the controlled object has to avoid the region of possible collisions, in a given time, with an uncontrolled target. This problem is translated into a min-max problem and solved with a memetic algorithm.[6]

As an illustrative example, the paper presents the case of an object moving on a circular low-Earth orbit and subject to a significant unmodelled acceleration component proportional to the square of the velocity.

QUANTIFICATION OF MODEL UNCERTAINTY

Let $f : \mathcal{S} \times \mathcal{P} \times [t_0 : t_0 + T] \longrightarrow \mathbb{R}^n$ and $\nu : \mathcal{S} \times \mathcal{B} \times [t_0 : t_0 + T] \longrightarrow \mathbb{R}^n$ be two vectorial functions with $\mathcal{S} \subseteq \mathbb{R}^n$, $B \subset \mathbb{R}^{m_b'}$ and $\mathcal{B} \subset \mathbb{R}^{m_b}$, $n, m_b', m_b \in \mathbb{N}^+$. Consider the following initial value problem

$$\begin{cases} \dot{s} = f(s, b', t) + \nu(s, b, t) \\ s(t_0) = s_0 \end{cases} \tag{1}$$

where s is the state vector, the map $\nu(s, b, t)$ represents some unknown function of the states that is capturing all unmodelled components, $b' \in \mathcal{P} \subseteq \mathbb{R}^{m_b'}$ is a set of uncertain model parameters, $b \in \mathcal{B} \subseteq \mathbb{R}^{m_b}$ is some unknown parameter vector of the unmodelled components, and t is the time coordinate. In this paper, let us restrict ourselves to the case in which the unmodelled components are not a function of time (the case with time dependence is easily obtained from the time independent formulation). Furthermore, let us consider the special case in which the function ν can be expressed as

$$\nu_{p_h}(s, b) = 0, \quad \nu_{q_h}(s, b) = Q_h = \nabla_{p_h} U(s, b) + \nabla_{q_h} U(s, b) \tag{2}$$

for $h = 1, \ldots, N$, where $s = (p, q)^T \in \mathbb{R}^{2N}$ is the action and moment vector, $Q : \mathcal{S} \times \mathcal{B} \longrightarrow \mathbb{R}^N$, and U is a continuous and differentiable scalar uncertainty function that can be expanded in the following hierarchical form:

$$U(s, b) \simeq a(b)_0 + \sum_i^{2N} a(b)_i \xi_i(s_i)$$
$$+ \sum_i^{2N} \sum_j^{2N} a(b)_{ij} \xi_{ij}(s_i, s_j) + \sum_i^{2N} \sum_j^{2N} \sum_k^{2N} a(b)_{ijk} \xi_{ijk}(s_i, s_j, s_k) + \ldots \tag{3}$$

with $a(b)_0, a(b)_i, a(b)_{ij}, \ldots$ polynomials in the components of b only. If Eq. (1) describes the time evolution of a dynamical system, then Q can be seen as a generalised force whose h^{th}-component

is:

$$Q_h(s,b) = \frac{\partial U}{\partial s_h} \simeq \sum_i^{2N} a(b)_i + \sum_i^{2N} \zeta_i(s_i)$$

$$+ \sum_i^{2N} \sum_j^{2N} \zeta_{ij}(s_i, s_j) + \sum_i^{2N} \sum_j^{2N} \sum_k^{2N} \zeta_{ijk}(s_i, s_j, s_k) + \dots \tag{4}$$

with $\zeta_i = a(b)_{ih} \partial \xi_{ih}/\partial s_h + a(b)_{hi} \partial \xi_{hi}/\partial s_h$, for $i = 1, \dots, 2N$, and so on. If ξ are monomial bases, then the generalised force reads:

$$Q_h(s,b) \simeq c_0 + \sum_i^{2N} c(b)_i \Delta s_i$$

$$+ \sum_i^{2N} \sum_j^{2N} c(b)_{ij} \Delta s_i \Delta s_j + \sum_i^{2N} \sum_j^{2N} \sum_k^{2N} c(b)_{ijk} \Delta s_i \Delta s_j \Delta s_k + \dots \tag{5}$$

with $c_0 = \sum_i^{2N} a(b)_i$ and $c(b)_i, c(b)_{ij}, \dots$ polynomials in b. Let us indicate with $l \in \mathbb{N}^+$ the dimension of the vector $c = (c_0, c(b)_1, \dots, c(b)_{2N}, c(b)_{11}, \dots)^T$.

Problem Statement

Given Q and a set of observations, one can obtain an approximated representation of the unmodelled components by finding the value of c that best fits the measurements. Then, the value of the coefficients of expansion (4) can be obtained as the solution of an optimisation problem. The nature of the optimisation problem slightly differs depending on the integration scheme used to solve Eq. (1). If N_o exact and distinct measurements are available then one needs to solve the set of constraints

$$s(t_i, c) - s_o(t_i) = 0, \qquad i = 1, \dots, N_o, \tag{6}$$

where $s(t_i, c)$ is the propagated state at time t_i and $s_o(t_i)$ is the observed state at time t_i. If the number of observations N_o is equal to l, the number of coefficients in expansion (4), one could argue that the solution of problem (6) provides the exact values of all the components of c. Constraint equations (6) can be solved in a least square sense by solving:

$$\min_c [s(t, c) - s_o(t)]^T [s(t, c) - s_o(t)] \tag{7}$$

Alternatively, if $N_o < l$, a suitable smoothing function can be introduced and the following problem needs to be solved:

$$\begin{aligned} \min_c \ & J(s, c) \\ \text{s.t.} \quad & s(t_i, c) - s_o(t_i) = 0, \quad i = 1, \dots, N_o, \end{aligned} \tag{8}$$

where $J : \mathcal{S} \times \mathcal{C} \longrightarrow \mathbb{R}$ is a real function of states $s \in \mathcal{S} \subset \mathbb{R}^n$ and coefficients $c \in \mathcal{C} \subset \mathbb{R}^l$. Note that, in general, problem (8) can have more than one solution for c, even when $N_o = l$.

3

Treatment of Stochastic Observations

The interest in this paper is to reconstruct the missing components from a small set of sparse observations over possibly long arcs. In the case of observations affected by an error, one cannot obtain a prediction of the exact value of the parameters c. In this case, it is reasonable to assume that the initial conditions are also uncertain as they come from previous observations. If the expected values of the state vector, coming from observations, are enforced as hard constraints the result might not capture the actual missing components as the trajectory is forced to satisfy constraints that do not come from the natural dynamics but are dependent on the errors in the observations. One option is to consider the most probable value for each observation and a cost function that maximises the likelihood of correct identification. The other option is to quantify the uncertainty in the observations and initial conditions as confidence intervals on the observed states. More formally, consider the uncertainty space $(\Gamma, \mathcal{L}, \mathcal{M})$, with Γ a non empty set, $\mathcal{L}$ a σ-algebra over Γ, and $\mathcal{M}$ an uncertainty measure. Then the observed state is an uncertainty variable $s_o : (\Gamma, \mathcal{L}, \mathcal{M}) \longrightarrow \mathbb{R}^n$. If the distribution of s_o is available, one can draw N_p samples and solve problem (8) N_p times to derive a distribution of the coefficients c. Alternatively, if no distribution is available for s_o, but Σ is the collection of all the confidence intervals for all the observations, including the initial conditions, such that

$$Pr(s_o \in \Sigma) > \varepsilon, \tag{9}$$

with $\varepsilon > 0$, then one can formulate the following optimisation problem:

$$\begin{aligned} \min_{c \in \mathcal{C}} \ & J(s, c) \\ \text{s.t.} \ & s(t_i) \in \Sigma, \quad i = 0, \ldots, N_o. \end{aligned} \tag{10}$$

The main advantage of this formulation is that no statistical moments are required, and no exact distribution needs to be known a priori. Note that the initial conditions $s(t_0)$ are treated as an observed state.

The objective function in Eq. (10) can be interpreted as a distance in the metric vector space $\mathcal{C}$ of the parameters c. In this space, the origin represents the solution with no model uncertainty and any point at distance $\sqrt{c^T c}$ from the origin has uncertainty vector Q and *uncertainty distance*:

$$d_u = \int Q^T Q \, dt. \tag{11}$$

MODEL UNCERTAINTY IN ORBITAL DYNAMICS

As an example, we take the case of a spacecraft in low-Earth orbit. The gravity component of the model is fully known, but the observations show an additional component that is not modeled. The real dynamics is governed by the following system of differential equations written in Hill's variables:[7]

$$\begin{aligned} \dot{r} &= v_r \\ \dot{u} &= G/r^2 - r \cos I \sin u F_n / (G \sin I) \\ \dot{h} &= r \sin u F_n / (G \sin I) \\ \dot{v}_r &= G^2/r^3 - \mu/r^2 + F_r \\ \dot{G} &= r F_u \\ \dot{H} &= r \cos I F_u - r \sin I \cos u F_n \end{aligned} \tag{12}$$

where F_r, F_u, F_n are the component of the non-gravitational forces in the radial, transversal, and out-of-plane reference frame.

The Hill variables $\{r, u, h, v_r, G, H\}$ are canonical variables introduced into satellite orbit theory by Izsak[7] in 1963. They represent, respectively, the radial distance, the argument of pericentre, the longitude of the ascending node, the radial velocity, the absolute value of the angular momentum, and the z-component of the angular momentum. The elements are illustrate in Figure 1.
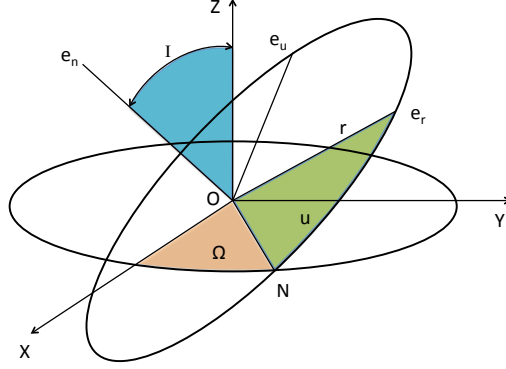
Figure 1: Reference frame (e_r, e_u, e_n)

The governing equations (12) can be re-written in the following form that explicitly introduces the transversal velocity v_u, with $v_u = G/r$:

$$\dot{r} = v_r$$
$$\dot{u} = v_u/r - r\cos I \sin u F_n/(rv_u \sin I)$$
$$\dot{h} = r\sin u F_n/(rv_u \sin I) \qquad (13)$$
$$\dot{v}_r = v_u^2/r - \mu/r^2 + F_r$$
$$\dot{v}_u = F_u - v_r v_u/r$$
$$\dot{H} = r\cos I F_u - r\sin I \cos u F_n$$

In our example, the non-gravitational force is $F = -C_d|v|v$, with $|v|^2 = v_r^2 + v_u^2$, and $v_n = 0$. We assume a constant value for $C_d = 0.5 \cdot 10^{-6}$ km^{-1} so that an appreciable variation of the orbit is obtained already after one orbit. Furthermore, we assume that the measured variation is with respect to a nominal circular orbit with $v_r(t = 0) = v_{r_0} = 0$ and $v_u(t = 0) = v_{t_0}$. The orbital period, without unmodelled force, is $T = 2\pi\sqrt{r^3/\mu}$. Substituting the expression of F in Eqs. (13), the vectorial field becomes

$$\dot{r} = v_r$$
$$\dot{u} = v_u/r$$
$$\dot{h} = 0 \qquad (14)$$
$$\dot{v}_r = v_u^2/r - \mu/r^2 - C_d|v|v_r$$
$$\dot{v}_u = -C_d|v|v_u - v_r v_u/r$$
$$\dot{H} = -r\cos I\, C_d|v|v_u$$

5

In order to capture the unmodelled dynamics, we consider an expansion of Q of the following form

$$
\begin{aligned}
Q_r &= c_1 + c_3 r + c_5 r^2 + c_7 ru + c_9 v_r + c_{11} v_r^2 + c_{13} v_r v_u \\
Q_u &= c_2 + c_4 u + c_6 u^2 + c_8 ru + c_{10} v_u + c_{12} v_u^2 + c_{14} v_r v_u \\
Q_n &= 0
\end{aligned}
\tag{15}
$$

where Q_n is zero because it is assumed that the unmodelled component acts only in-plane, and $c_i \in \mathbb{R}, i = 1, \ldots, 14$. Equation (15) is an incomplete expansion of (5) when the generalised potential U in (3) is truncated at the third order. The vectorial field (14) is then expanded as

$$
\begin{aligned}
\dot{r} &= v_r \\
\dot{u} &= v_u/r \\
\dot{h} &= 0 \\
\dot{v_r} &= v_u^2/r - \mu/r^2 + c_1 + c_3 r + c_5 r^2 + c_7 ru + c_9 v_r + c_{11} v_r^2 + c_{13} v_r v_u \\
\dot{v_u} &= c_2 + c_4 u + c_6 u^2 + c_8 ru + c_{10} v_u + c_{12} v_u^2 + c_{14} v_r v_u - v_r v_u/r \\
\dot{H} &= r \cos I (c_2 + c_4 u + c_6 u^2 + c_8 ru + c_{10} v_u + c_{12} v_u^2 + c_{14} v_r v_u)
\end{aligned}
\tag{16}
$$

If the linear effects in Eq. (14) are dominant over a given time span Δt, and there is no out-of-plane component, then the prediction given by Eq. (16) should be of the form:

$$
\begin{aligned}
\dot{r} &= v_r \\
\dot{u} &= v_u/r \\
\dot{h} &= 0 \\
\dot{v_r} &= v_u^2/r - \mu/r^2 + c_{13} v_r v_u \\
\dot{v_u} &= -v_u v_r/r + c_{12} v_u^2 \\
\dot{H} &= r \cos I \, c_{12} v_u^2
\end{aligned}
\tag{17}
$$

We can now introduce observations at time $t = T$ and $t = T/2$, for a total of 8 constraint equations and 14 parameters. If measurements are affected by an error, problem (10) needs to be solved under some assumptions on the initial conditions. The assumption in this paper is that the initial conditions are taken over a given interval. The size of the confidence on each state variable for the initial conditions and for each observation is $r \in [\bar{r} - 0.01, \bar{r} + 0.01]$ km, $u \in [\bar{u} - 10^{-5}, \bar{u} + 10^{-5}]$ rad, $h \in [\bar{h} - 10^{-5}, \bar{h} + 10^{-5}]$ rad, $v_r \in [\bar{v}_r - 10^{-5}, \bar{v}_r + 10^{-5}]$ km/s, $v_u \in [\bar{v}_u - 10^{-5}, \bar{v}_u + 10^{-5}]$ km/s, $H \in [\bar{H} - 10^{-5}, \bar{H} + 10^{-5}]$ km^2/s, which is consistent with a good orbit determination process, where $\bar{r}, \bar{u}, \bar{h}, \bar{v}_r, \bar{v}_u, \bar{H}$ are the exact values.

The estimated c parameters are represented in Figure 2 together with their associated confidence intervals. As one can see, the expected value is close to the expected true solution. One thing that has to be taken into consideration is that the dynamics that are simulated and measured are the true dynamics, not the approximated equations (14). Therefore, some components that are not in the approximated model (14) might be different from zero.

Note that the values of all the coefficients in the figures are normalised by $0.5 \cdot 10^{-6}$. The $\mathcal{C}$ space in this case has boundaries $[-10^{-5}, 10^{-5}]$ for all the coefficients. As one can see, even if a linear model is assumed, the prediction of the coefficient is very good with some relevant uncertainty on coefficient $c_1, c_2, c_4, c_9, c_{10}, c_{13}, c_{14}$. Given the predicted values of the coefficients one can now
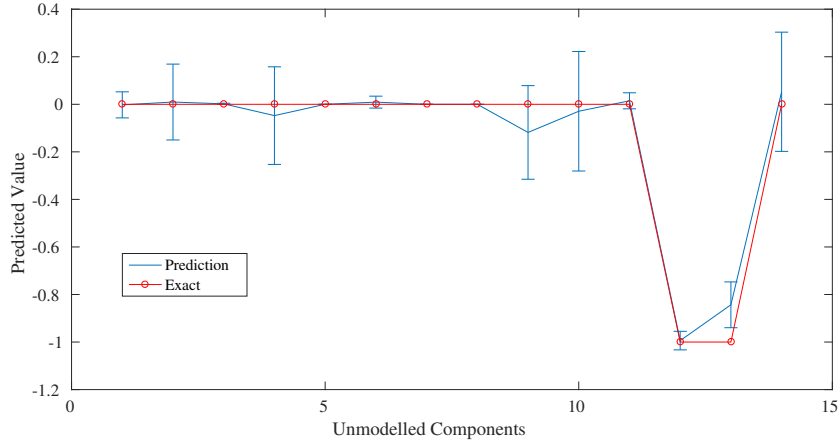
Figure 2: Example of reconstructed gravity-drag dynamics with confidence intervals

predict the future evolution of the orbit over another period. The resulting trajectory over two orbits is shown in Figures 3.

The match between the predicted and the true trajectory is very good although a 2 km error in radius accumulated by the end of the second orbit. Once a first estimation of the coefficient is available, one can iterate the process progressively removing the coefficients that fall below a given threshold. Given the result in Figure 2, one can take all the coefficients with an absolute mean value higher than 0.1 and solve problem (10) once again. From Figure 2 coefficients c_9, c_{12} and c_{13} can be retained, and Eqs. (16) becomes:

$$
\begin{aligned}
\dot{r} &= v_r \\
\dot{u} &= v_u/r \\
\dot{h} &= 0 \\
\dot{v_r} &= v_u^2/r - \mu/r^2 + c_9 v_r + c_{13} v_r v_u \\
\dot{v_u} &= c_{12} v_u^2 - v_r v_u/r \\
\dot{H} &= r \cos I \, c_{12} v_u^2
\end{aligned}
\tag{18}
$$

After solving problem (10) only with three coefficients, the result is represented in Figure 4. Even in this case after predicting the dynamics over one orbit, one can study the evolution over a second orbit. The absolute error between predicted and true trajectory can be seen in Figure 5.

A REACHABILITY PROBLEM

Once the reachable sets of the controlled and uncontrolled objects are available, a collision avoidance maneuver is calculated solving the following min-max optimal control problem:
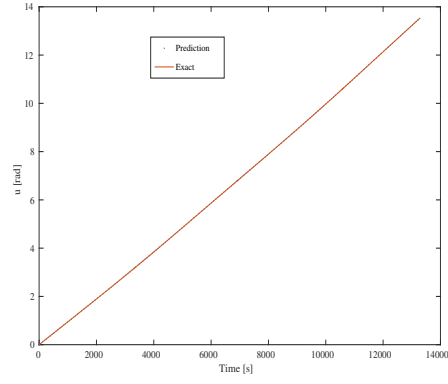
$$
\begin{aligned}
&\min_{w \in \mathcal{A}} \max_{c \in \Xi} \psi(s(t_f), w, c, t_f) \\
\text{s.t} \quad &\dot{s} = f(s, p) + \nu(s, b) + g(s, w) \\
&s(t_0) \in \Sigma_0
\end{aligned}
\tag{19}
$$

where ψ is a real function, Σ_0 is the set of possible initial conditions, Ξ is the set in which the components of the coefficient vector c are defined, ν is an approximation of the unmodelled components
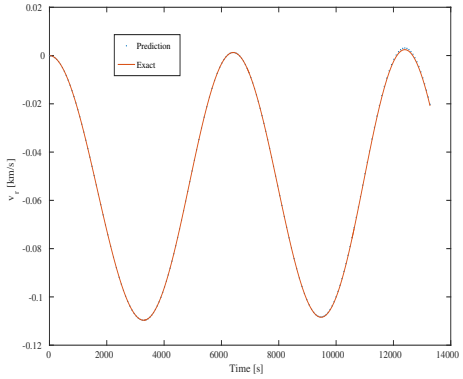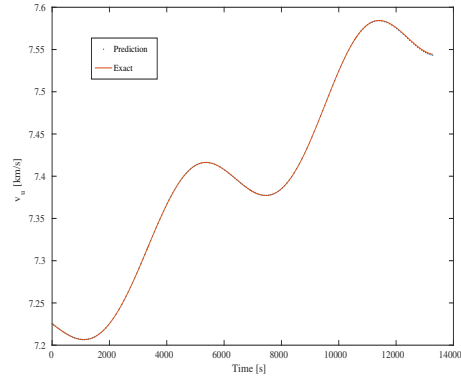
7
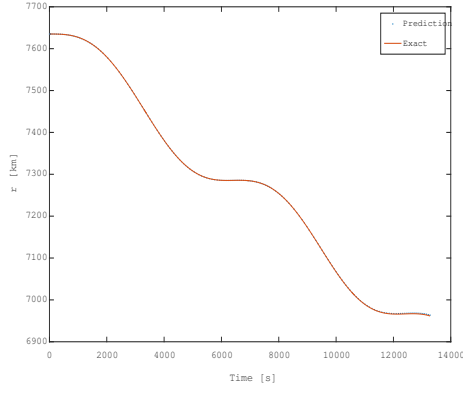
(a) Component r

(b) Component u

(c) Component v_r

(d) Component v_u

Figure 3: Comparison between the true and predicted estimates.

in the dynamics given by Eqs. (2)–(3), g is the control function, and $\mathcal{A}$ is the space of admissible controls. The function $\psi(s(t_f), w, c, t_f)$ defines whether the terminal state is admissible or not. In other words the reachable set is defined by a level set of ψ.

Artificial potential

Since the interest is to avoid a collision the desired reachable set is the space outside the uncontrolled target. Thus the function ψ has to be negative or null when a collision occurs and strictly positive otherwise. We started from a tessellation of the region describing the object. A tessellation is a tiling of the space using one or more geometrical shapes, called tiles, with no overlaps and no gaps. An example is a tiling with cubes. Let U be the region to cover and $D_1, \ldots, D_m$ the polyhedra used as tiles. Let n be the dimension of the space and $q > n + 1$ be the number of facets of the polyhedron. We are assuming that the polyhedra in the tessellation are of the same type, however, our dissertation can be extended to the case of a tessellation with different polyhedra.

Each facet can be represented by an hyperplane of equation $A_k^{(j)} \cdot (x - x_j) = b_k^{(j)}$, with $A_k^{(j)} \in \mathbb{R}^q, b_k^{(j)} \in \mathbb{R}^q$, and $x_j \in \mathbb{R}^n$ is the center of the j-th polyhedron. The sign of $A_k^{(j)}, b_k^{(j)}$ are such that
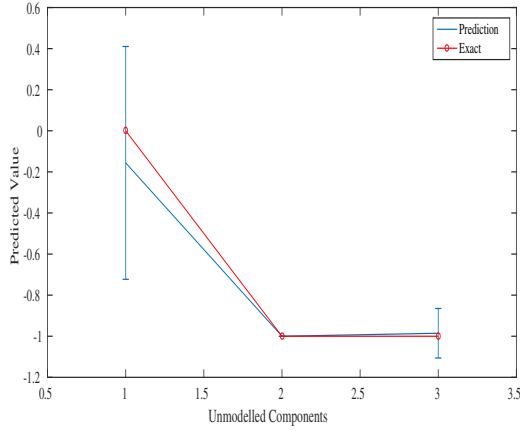
Figure 4: Prediction of the coefficients for the reduced model

the semi-plane $A_k^{(j)} \cdot (x - x_j) \leq b_k^{(j)}$ contains the center x_j for each k, j. Indicating with $\mathcal{K}_j$ the set $\{k \; : \; A_k^{(j)} \cdot (x - x_j) - b_k^{(j)} > 0\}$, the function

$$
\phi_j(x) = \begin{cases} -\dfrac{1}{1 + ||x - x_j||^3} \,, & \text{if } \mathcal{K}_j = \emptyset \,, \\ \displaystyle\sum_{k \in \mathcal{K}_j} (A_k^{(j)}(x - x_j) - b_k^{(j)}) \,, & \text{otherwise} \,, \end{cases}
\tag{20}
$$

is such that $\phi_j(x) > 0$ if x is outside every semi-plane, that is outside D_j, and it is $\phi_j(x) \leq 0$ if x is inside or on the border of D_j. We note that function (20) is discontinuous on the border of D_j, however, continuity is not a requirement for our study. We call ϕ_j artificial potential of D_j. An example is shown in Figure 6.

Using the tessellation, the set U is approximated with the union of disjoint sets $D_j, j = 1, \ldots, m$, and the artificial potential on this set is defined as

$$
\Phi(x) = \begin{cases} -\displaystyle\sum_{j=1}^{m} \dfrac{1}{1 + ||x - x_j||^3} \,, & \text{if } \mathcal{K}_j = \emptyset \text{ for some } j \\ \displaystyle\sum_{j=1}^{m} \sum_{k \in \mathcal{K}_j} (A_k^{(j)}(x - x_j) - b_k^{(j)}) \,, & \text{otherwise} \end{cases}
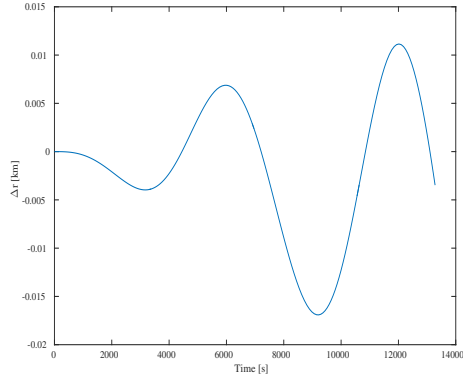\tag{21}
$$

and satisfies the requirement:

$$
\Phi(x) = \begin{cases} \leq 0 \,, & \text{if } x \in D_1 \cup \ldots \cup D_m \,, \\ > 0 \,, & \text{otherwise} \,. \end{cases}
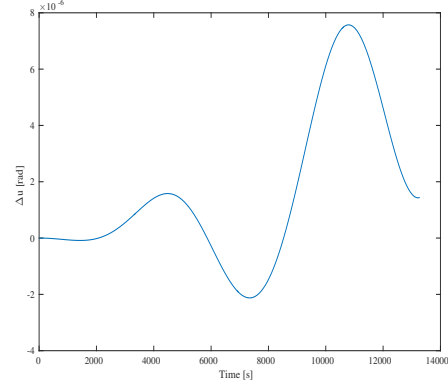\tag{22}
$$

Superquadratic functions can be used as an alternative to the use of hyperplanes:

$$
\varphi_j \; : \; \left\| x_1 - x_1^{(j)} \right\|^{r_1} + \ldots + \left\| x_n - x_n^{(j)} \right\|^{r_n} - 1 \,,
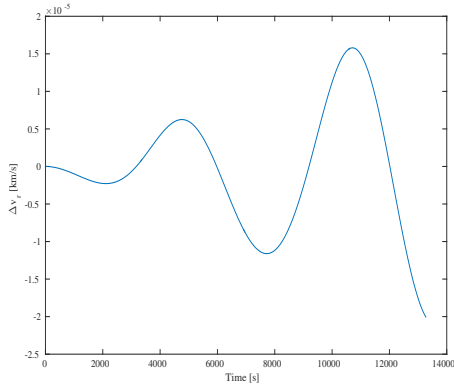\tag{23}
$$

where $x_j = (x_1^{(j)}, \ldots, x_n^{(j)})$ is the center of D_j, and $r_1, \ldots, r_n$ are positive real numbers. For $r_i = 1, i = 1, \ldots, m$, the superquadratic represents an hypercube. Or, in a three-dimensional space,
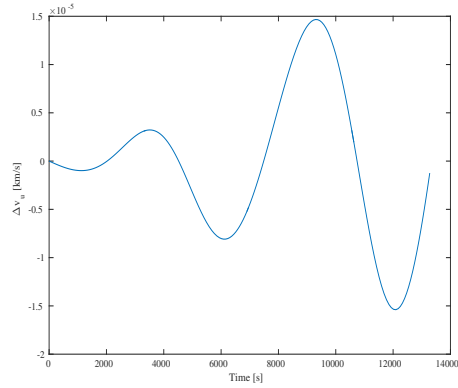
9

(a) Component r (b) Component u

(c) Component v_r (d) Component v_u

**Figure 5**: Difference between the true and predicted estimates.

one could use the superellipsoid

$$\varphi'_j \ : \ \left(\left\| x_1 - x_1^{(j)} \right\|^r + \left\| x_2 - x_2^{(j)} \right\|^r \right)^{t/r} + \left\| x_3 - x_3^{(j)} \right\|^t - 1 \,, \tag{24}$$

with r, t real numbers that depends on x_j. Then, we set

$$\Phi(x) = \begin{cases} - \displaystyle\sum_{j=1,\dots,m} \dfrac{1}{1 + \|x - x_j\|^3} \,, & \text{if } \varphi_j \circ \tau_j(x) \leq 0 \text{ for some } j \\ \displaystyle\sum_{j=1,\dots,m} \varphi_j(x) \,, & \text{otherwise} \,, \end{cases} \tag{25}$$

and the condition (22) is still satisfied. The transformation τ_j in Eq. (21) represents the change of coordinates that rotates and scales the basic shape of the polyhedron D_j into a superquadratic equation of the form (23). The function ψ is taken as the artificial potential Φ.

(a)   (b)
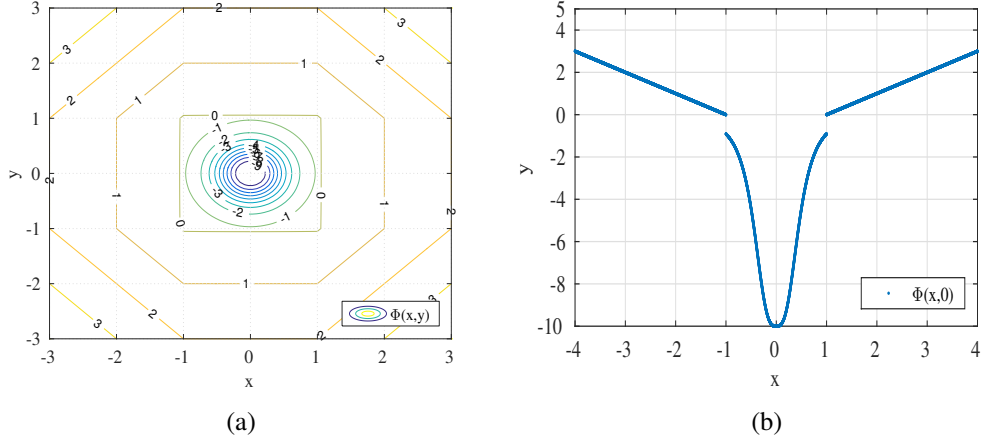
Figure 6: Level curves of the pesudo potential on the cube $[-1, 1]^2$ (a) and the corresponding values along the x-axis

Solution Approach

The algorithm proposed in this paper to solve min-max problem (19) is a combination of the one proposed in Vasile[6] and Marzat et al.[8] In Marzat,[8] the generic unconstrained min-max problem:

$$\min_{d \in \mathcal{D}} \max_{\xi \in \mathcal{U}} f(d, \xi)$$

is computed by solving iteratively the following two problems, one after the other:

$$\xi_a = \text{argmax}_{\xi \in \mathcal{U}} f(d_{min}, \xi) \tag{26}$$

$$d_{min} = \text{argmin}_{d \in \mathcal{D}} \left\{ \max_{\xi_a \in A_\xi} f(d, \xi_a) \right\} \tag{27}$$

where the archive A_ξ is a collection of all the ξ_a generated by the solution of problem (26) for each new d_{min} generated by the solution of problem (27). Problem (26) can be seen as a restoration of the maximum condition on $\mathcal{U}$, therefore the whole process can be considered as a *minimisation-restoration* loop.

It is important, at this point, to observe that, if a population-based method is used to solve problem (27), subproblem $\max_{\xi_a \in A_\xi} f(d, \xi_a)$ can be interpreted as a cross-check of the ξ associated to a population P of d values as in Vasile.[6] For each d, in fact, problem (27) requires selecting the $\xi_{a,max}$ that maximizes f among all the ξ_a found thus far. This principle is equivalent to the Nash ascendancy relationship in game theory used in Dumitrescu et al.,[9] as it corresponds to selecting the best strategy, among all the ones that the players in the population P can play. In the scheme proposed by Marzat,[8] however, the minimisation over $\mathcal{D}$ is performed assuming that the elements in the archive are not updated while f is minimised over $\mathcal{D}$. The main consequence is that convergence can be achieved if the archive A_u contains a sufficient number of elements. In Vasile[6] instead the solutions were recalculated either running a global or a local optimisation as d was changing. The main reason for the latter strategy is that a variation of d, seen from the space $\mathcal{U}$, can correspond to a change in the location of the maxima. When this occurs the solution of problem (27) can lead to values of d_{min} such that the maximum of f over A_ξ is very far even from a local optimum.

The whole process, therefore, might iterate for a long time between minimization and restoration without converging. This is what can be called *red queen effect*.

Here, it is proposed to solve both problems (26) and (27) with Inflationary Differential Evolution Algorithm (IDEA)[10] and to allow the algorithm to compute for each d a local maximum $\xi^*_{a,max}$ starting from each element in A_ξ. The value d_{min} with associated local maximum $\xi^*_{a,max} = \mathrm{argmax}_{\xi^*_a \in \mathcal{U}} f(d_{min}, \xi^*_a)$, are then saved in the archive A_d and the elements in the archive A_d are cross-checked to maximise the change to identify the global maximum in $\mathcal{U}$. The overall strategy is presented in Algorithms 1, 2, and 3.

Algorithm 1 IDEA$minmax$

Initialize $\bar{d}$ at random and run $\xi_a = \mathrm{argmax}_{\xi \in \mathcal{U}} f(\bar{d}, \xi)$
$A_\xi = A_\xi \bigcup \{\xi_a\}$
while $n_{feval} < n_{feval,max}$ **do**
    Run $d_{min} = \mathrm{argmin}_{d \in \mathcal{D}} \{\max_{\xi^*_a \in A^*_\xi} f(d, \xi^*_a)\}$
    Run $\xi_a = \mathrm{argmax}_{\xi \in \mathcal{U}} f(d_{min}, \xi)$
    if $f(d_{min}, \xi^*_{a,max}) < f(d_{min}, \xi_a)$ **then**
        $A_\xi = A_\xi \bigcup \{\xi_a\}$, $A_d = A_d \bigcup \{d_{min}, \xi_a\}$
    else
        $A_\xi = A_\xi \bigcup \{\xi^*_{a,max}\}$, $A_d = A_d \bigcup \{d_{min}, \xi^*_{a,max}\}$
    end if
end while
Run Cross Check Algorithm 3 over the archive A_d

Algorithm 2 $\max_{\xi^*_a \in A^*_\xi} f(d, \xi^*_a)$

---

for all the elements in A_ξ **do**
    Run local search from $\xi_a \in A_\xi$ and compute $\xi^*_a = \mathrm{argmax}_{\xi \in \mathcal{U}} f(d_{min}, \xi)$
    Add local maximum to the set of local maxima $A^*_\xi = A^*_\xi \bigcup \{\xi^*_a\}$
end for
$\xi^*_{a,max} = \mathrm{argmax}_{\xi^*_a \in A^*_\xi} f(d_{min}, \xi^*_a)$

Algorithm 3 Cross Check

Initialize $\Delta, \varepsilon > 0$
while $\Delta > \varepsilon$ **do**
    for all the elements in A_d **do**
        Compute local maximum $f(d_i, \xi^*_j)$ from $\xi_j \in A_d$
        $\Delta = f(d_i, \xi^*_j) - f(d_i, \xi_i)$
        if $\Delta > \varepsilon$ **then**
            $\xi_i = \xi^*_j$
        end if
    end for
end while

Numerical Examples

For the sake of illustrating the approach proposed in the previous sections, we consider the case in which after the identification of the missing component, a manoeuvre is required to avoid the collision with a known, though uncontrolled object. We say that a collision occurs when the artificial potential in Eq. (21) is non-positive. For this exercise we consider the position of the two objects projected onto the b-plane at the expected time of impact. The impact occurs almost one orbit after the last measurement is acquired. A low-thrust manoeuvre is then applied to avoid the collision. Since a negative artificial potential corresponds to a collision and a positive artificial potential corresponds to no collision, the problem translates into finding the optimal control profile that maximises the artificial potential (21). At the same time, given the uncertainty on the coefficients c, an optimal and robust control policy has to account for the worst-case value of c.

The reachability problem then reads:

$$
\begin{aligned}
\min_{w \in \mathcal{W}} \max_{c \in \Xi} \ & \psi(r, u, h, v_r, v_u, H, w, c, t_i, t_f) \\
\text{s.t.} \quad \dot{r} &= v_r \\
\dot{u} &= v_t/r - \cos I \sin u \, w_n/(v_u \sin I) \\
\dot{h} &= \sin u w_n/(v_u \sin I) \\
\dot{v_r} &= v_u^2/r - \mu/r^2 + c_1 v_r + c_3 v_r v_u + w_r \\
\dot{v_u} &= c_2 v_u^2 - v_r v_u/r + w_u \\
\dot{H} &= r \cos I (c_2 v_u^2 + w_u) - r \sin I \cos u w_n \\
s(t_0) &\in \Sigma_0
\end{aligned}
\tag{28}
$$

where $(r, u, h, v_r, v_u, H)^T$ are the Hill variables, $w = (w_r, w_u, w_n)$ is the control acceleration, $c = (c_1, c_2, c_3)$ are the unknown coefficients in the dynamics, and t_i, t_f are a generic instant of time and the final time, respectively. The control acceleration is the decision vector w described in the previous section, and the c is the uncertain vector ξ. Each component of the control acceleration is modeled as a fourth order polynomial, collocated at five points in time along the trajectory. The differential equations in (28) are integrated forward in time with a Runge-Kutta 4/5 order scheme with variable step size.

Figure 7 shows the uncertainty region of the controlled object due to the uncertainty on the coefficients c_1, c_2, c_3 and initial conditions. Before the manoeuvre, the projection of the uncontrolled object on the target plane is in the origin of axis, and the level curves of the artificial potential are shown in Figure 8. We considered two cases, one in which the admissible control space $\mathcal{W}$ is a box with edge $[-10^{-5}, 10^{-5}]$ m/s^2, the other in which the edge is $[-4 \times 10^{-6}, 4 \times 10^{-6}]$ m/s^2. The propagation of the position is given in Figure 9, where we also observe that the low-trust (thick solid line) is on for half period, and it has the effect to lower the radial distance.

FINAL REMARKS

We proposed a method to derive a robust control policy to avoid a collision between a controlled object and an uncontrolled target when the dynamics of the controlled object is affected by model uncertainty. The missing components of the dynamics are approximated with a polynomial expansion. The upper and lower bounds for the coefficients of the polynomial expansion are determined using sparse observations. Once the uncertainty model is quantified, an optimal low-thrust control policy that maximises the minimum possible distance between the controlled object and the target, is computed solving a min-max optimal control problem.
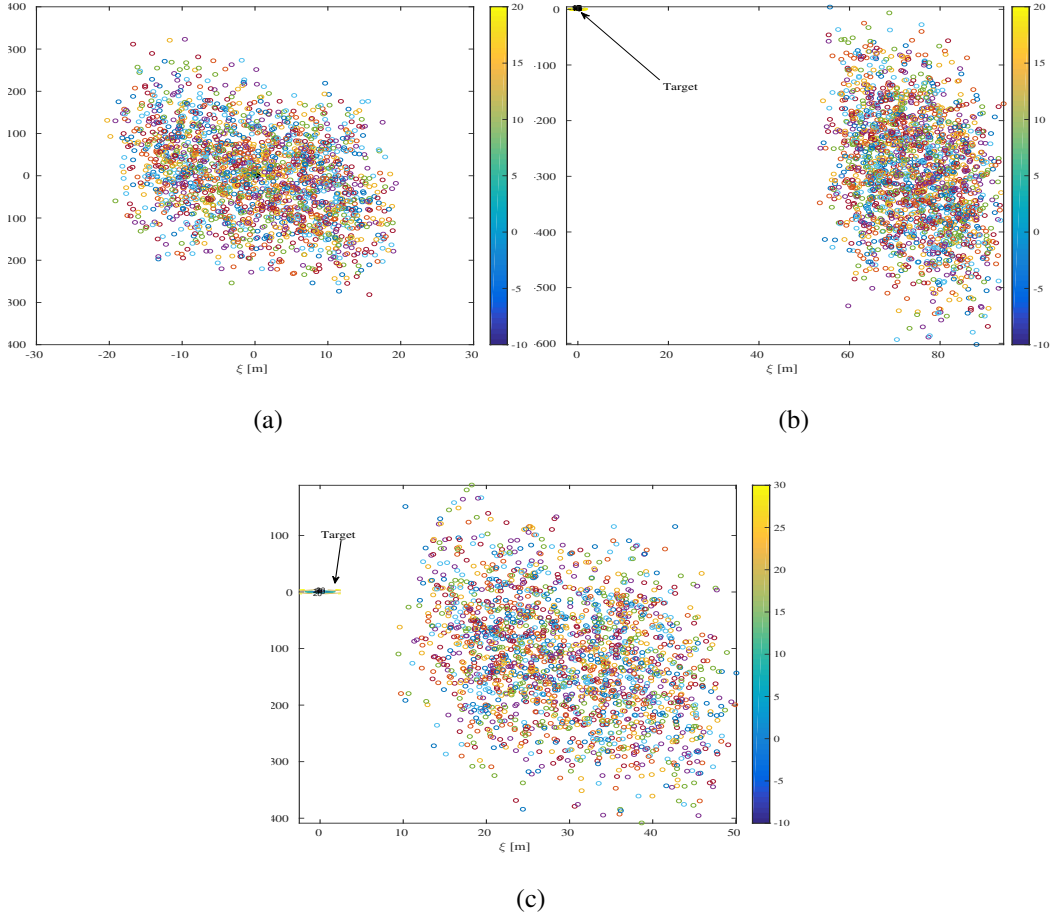
Figure 7: Uncertainty region on the b-plane: (a) no manoeuvre (b) post-manoeuvre with maximum acceleration along each component of 10^{-5} m/s^2 (c) post-manoeuvre with maximum acceleration along each component of 4×10^{-6} m/s^2

The use of polynomial expansions is reminiscent of the use of polynomial chaos expansions in multifidelity modeling to represent discrepancies in the model. This form of polynomial representation was demonstrated to well capture the missing part of the dynamics in the case of a circular orbit and a force component proportional to the square of the orbital velocity. Note that exact distribution needs to be known a priori on boundary conditions and observed states.

Besides, once the predicted dynamics is available, the reachable set of an uncontrolled object at different times $t \in [t_o, t_f]$ can be approximated with one of the techniques proposed in Ricciardi et al.,[11] starting from the level set of an artificial potential. Likewise, the reachable set of a controlled object can be computed for the same time interval to assess the probability of a collision. In this way, the computation time is drastically reduced, especially in the optimisation part.

ACKNOWLEDGMENT

14
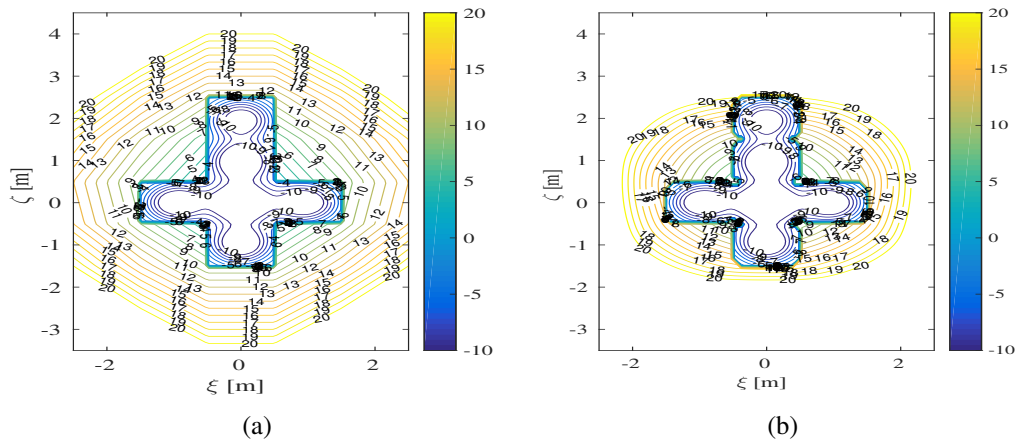
Figure 8: Level curves of the pesudo potential for: (a) a cross built with cubes projected on the b-plane (b) a cross built with super-ellipses projected on the b-plane

number L15548.

REFERENCES

[1] E. M. Alessi, S. Cicalo, and A. Milani, "Accelerometer Data Handling for the BepiColombo Orbit Determination," *Advances in the Astronautical Sciences*, Vol. 145, 2012, pp. 121–129.

[2] O. Montenbruck, T. Helleputte, R. Kroes, and E. Gill, "Reduced dynamic orbit determination using GPS code and carrier measurements," *Aerospace Science and Technology*, Vol. 9, 2005, pp. 261–271.

[3] L. W. T. Ng and M. S. Eldred, "Multifidelity Uncertainty Quantification Using Non-Intrusive Polynomial Chaos and Stochastic Collocation," *Proceedings of the 53rd AIAA/ASME/ASCE/AHS/ASC Structures, Structural Dynamics and Materials Conference, Honolulu, Hawaii*, 23-26 April 2012. AIAA 2012-1852.

[4] D. Giza, P. Singla, and M. Jah, "An Approach for Nonlinear Uncertainty Propagation: Application to Orbital Mechanics," *AIAA Guidance, Navigation, and Control Conference*, Chicago, Illinois, USA, 10-13 August 2009 2009.

[5] I. Hwang, D. Stipanovic, and C. Tomlin, "Polytopic Approximations of Reachable Sets Applied to Linear Dynamic Games and a Class of Nonlinear Systems," *Advances in Control, Communication Networks, and Transportation Systems*, 2005, pp. 3–19.

[6] M. Vasile, "On the solution of min-max problems in robust optimization," *The EVOLVE 2014 International Conference, A Bridge between Probability, Set Oriented Numerics, and Evolutionary Computing*, Beijing, July 2014.

[7] I. G. Izsak, "A Note on Perturbation Theory," *Astron. J.*, Vol. 68, Oct. 1963, pp. 559–561, 10.1086/109180.

[8] J. Marzat, E. Walter, and H. Piet-Lahanier, "A new strategy for worst-case design from costly numerical simulations," *American Control Conference (ACC), 2013*, June 2013, pp. 3991–3996.

[9] D. D. Dumitrescu, R. I. Lung, and T. D. Mihoc, "Meta-Rationality in Normal Form Games," *International Journal of Computers Communications & Control*, Vol. 5, No. 5, 2010.

[10] M. Vasile, E. Minisci, and M. Locatelli, "An inflationary differential evolution algorithm for space trajectory optimization," *IEEE Transactions on Evolutionary Computation*, 2011.

[11] A. Riccardi, C. Tardioli, and M. Vasile, "An intrusive approach to uncertainty propagation in orbital mechanics based on Tchebycheff polynomial algebra," *AAS Astrodynamics Specialists Conference, Vail, Colorado, USA, August 9–13*, 2015. AAS 15-544.
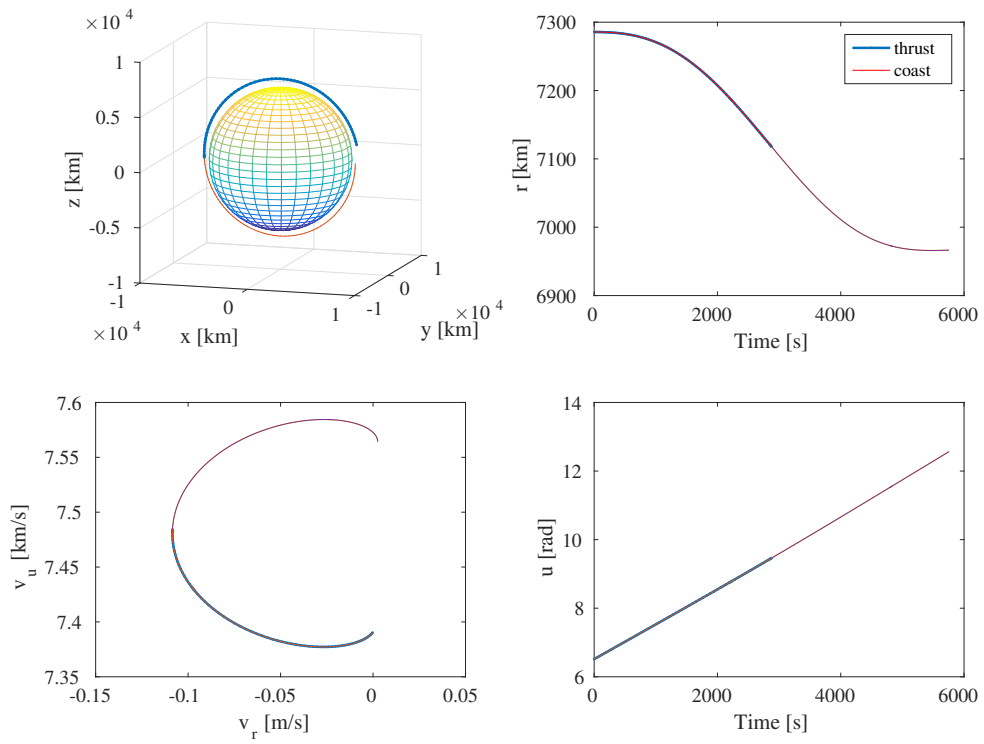
Figure 9: Evolution of the second orbit